Advances in Aerodynamics

RESEARCH

Open Access

Analysis of wind pressure characteristics of typical agricultural greenhouse buildings on tropical islands

Bin Huang[1*], Jinke Liu[1], Zhengnong Li[2], Wenxiang Wang[1], Xiangjun Wang[3], Xijie Liu[1] and Tianyin Xiao[1]

*Correspondence:
huangbin@hainanu.edu.cn

[1] School of Civil Engineering and Architecture, Hainan University, Haikou 570228, China
[2] Key Laboratory of Building Safety and Energy Efficiency of the Ministry of Education, Hunan University, Changsha 410082, China
[3] College of Electrical, Energy and Power Engineering, Yangzhou University, Yangzhou 225127, China

Abstract

Existing studies about wind pressure on agricultural greenhouse buildings concentrate on the mean wind pressure while ignoring the systematic research on fluctuating wind pressure characteristics and the influence of roof shape on the wind pressure characteristics, which are closely associated with the wind-induced damage mechanism. In this study, two typical agricultural greenhouse buildings on tropical islands are selected as prototypes to conduct pressure measurement experiments in the wind tunnel. Based on the wind pressure time series for the two greenhouses, the mean and fluctuating wind pressure distribution pattern and the localized high-pressure generation mechanism are analyzed. Then, the shape coefficient of the two greenhouses is compared in depth to the standards from four countries. Besides, wind pressure non-Gaussian determination criteria for agricultural greenhouse buildings considering the roof shape and wind directions are proposed. Lastly, the differences in wind pressure spectra on the roofs and walls of the two greenhouses are summarized. The results indicate the roof shape has a significant influence on the wind pressure characteristics. Compared with the pitched roof, the vaulted roof will increase the suction effect on the windward front zone and the middle area, mitigate the suction impact on the leeward roof, and weaken the wind pressure non-Gaussian characteristics. The experimental shape coefficient of the pitched-roof greenhouse is basically consistent with the standard from the U.S., while that of the vaulted-roof greenhouse has some deviation from the existing standards. The results provide a theoretical basis for the wind-resistant design of agricultural greenhouse buildings on tropical islands.

Keywords: Tropical island, Agricultural greenhouse building, Wind tunnel test, Wind load shape coefficient, Wind pressure characteristic, Wind pressure spectrum

1 Introduction

Agricultural greenhouse buildings are specific facilities that utilize light-transmitting covering materials and environmental control equipment to create optimal microclimates for crop growth and development. Influenced by the tropical maritime climate, agricultural greenhouse buildings in Hainan Province of China have suffered severe damage from the strong wind and typhoon [1]. The main reasons for the wind-induced damage are the poor understanding of the wind effects on greenhouse buildings on

tropical islands and the lack of standardized guidance for the wind-resistant design and construction of greenhouse buildings. Based on the above, wind pressure measurement tests of agricultural greenhouse buildings are performed in the wind tunnel, and the wind pressure characteristics and distribution patterns on the surface of the greenhouse buildings are summarized, which has significance against wind-induced disasters and reducing losses of agricultural greenhouse buildings on tropical islands.

According to the roof shape, the single-span greenhouse building could be mainly divided into the pitched-roof greenhouse and the vaulted-roof greenhouse. Previous studies on wind loads of agricultural greenhouse buildings were conducted by field measurement, wind tunnel test, and numerical simulation. Wells et al. [2] collected wind load data of glass greenhouses of five different cross-sections within 0°~90° by field measurement in the natural wind. Richardson et al. [3] measured the surface pressure of the greenhouse with and without shelter of 50% permeability in the natural wind and obtained the corresponding shelter factor. Kwon et al. [4] measured the wind pressure coefficients of four typical single-span greenhouses with different wind directions, roof slopes, and curvature radii in Korea by wind tunnel tests. Moriyama et al. [5, 6] conducted the wind pressure experiment using the 1:20 scale rigid model of a tube-shed greenhouse building to analyze the influence of sidehill wall openings on internal and external pressure coefficients and the influence of arrangement spacing on wind pressure coefficients of greenhouse buildings. Kim et al. [7] analyzed the design parameters of five greenhouse standards, including the specification of wind loads, correction factors, and shape coefficients, and summarized the differences among the standards. Besides, Kim et al. [8] analyzed the factors affecting the accuracy of numerical simulation, including the thickness of the atmospheric boundary layer, the turbulence model and the size of the computational domain. The reliability of numerical simulation is verified by comparing the simulation results with the wind tunnel results. Yang et al. [9] summarized wind pressure coefficient distribution patterns on the rigid model surface of the greenhouse building and deduced the critical wind speeds for various zones when wind-induced damage occurred. Xie et al. [10] carried out wind pressure experiments of a single plastic greenhouse in South China, analyzed the distribution pattern of wind load shape coefficients under 16 wind directions, and discussed the influence of the eave, skylight, and other extensions on the wind loads on the plastic greenhouse. Wu [11] conducted a wind tunnel test to analyze the distribution characteristics of wind pressure on the surface of greenhouse buildings with and without shade curtains. The results show that existing curtains can increase the wind pressure coefficient on the surface of greenhouse buildings.

In summary, existing studies about the wind effect of agricultural greenhouse buildings focus on the mean wind pressure on the surface of buildings while ignoring the systematic research on the statistical properties of the fluctuating wind pressure and the frequency domain characteristics. Based on the previous studies [12], the fluctuating wind pressure and the frequency domain characteristics are closely associated with the structural damage mechanism, which has vital theoretical and engineering significance to the wind-induced vulnerable greenhouse buildings. In addition, how the shape of the greenhouse roof influences the wind pressure distribution on the greenhouse building also deserves more scholarly research. It is necessary to lay the foundation for obtaining

the wind-induced damage mechanism of agricultural greenhouse buildings with different roof shapes.

In this study, rigid model pressure measurement experiments are conducted for agricultural greenhouse buildings with vaulted roofs and pitched roofs on tropical islands. Based on the collected wind pressure time series from the wind tunnel tests, firstly, this paper summarizes the distribution pattern of the mean and fluctuating wind pressure on the surface of two greenhouse buildings, then compares the shape coefficients with the standards from four countries, finally analyzes the influence of roof shape on the wind pressure non-Gaussian characteristics and fluctuating wind pressure spectra. The results provide a theoretical basis for the wind-resistant design of agricultural greenhouse buildings on tropical islands.

2 Wind tunnel tests

2.1 Modelling and pressure tap arrangement

Two typical single greenhouse buildings of an agricultural greenhouse base in Hainan Province of China are selected as research prototypes. The length of the greenhouses is 20 m, the width is 8 m, and the height is 5 m (3 m and 5 m at the eaves and the ridge, respectively). They are divided into vaulted-roof and pitched-roof greenhouses according to the roof shape. Figure 1 shows the geometric dimensions of the two roof models. The curvature radius of the vaulted-roof greenhouse is 5 m and the slope angle of the pitched-roof greenhouse is 26.6°. The geometry scale ratio of the rigid pressure-measurement model is 1:25 and the model is made of acrylonitrile–butadiene–styrene (ABS). The maximum blockage ratio of the test model is 2.3%, not exceeding 5% of the cross-sectional area, which meets the test requirements. Wind pressure measurement taps are installed on the surfaces of the wall and roof so that a detailed evaluation of wind pressure changes on the surface of the greenhouse building is possible. Considering the flow-separation zone where the strong suction and rapid change of the wind pressure make buildings more vulnerable to damage, dense taps are installed on the corner and verge zone of the models to capture detailed wind pressure changes [13].

Figure 2 shows the pressure tap distribution of the vaulted-roof and pitched-roof greenhouse models. The vaulted-roof model has a total of 419 pressure measurement taps (247 on the roof and 172 on the walls), and the pitched-roof model has a total of 432 pressure measurement taps (266 on the roof and 166 on the walls). Wind directions vary from 0° to 360° at intervals of 15°, and the test results at wind directions of 0° to 90° are under consideration because of the biaxial symmetry of the models. Because the Reynolds number of the vaulted-roof model is not completely consistent with that of

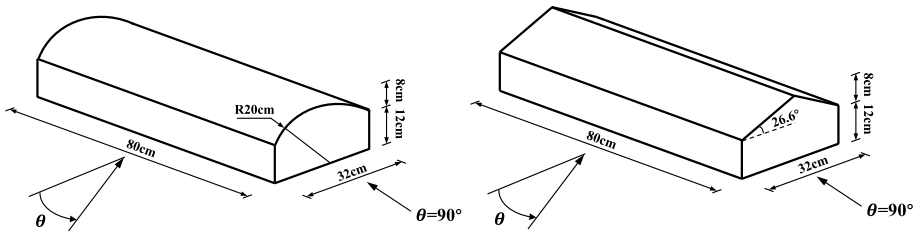

(a) Vaulted-roof model (b) Pitched-roof model

Fig. 1 Dimension of the pressure-measurement models

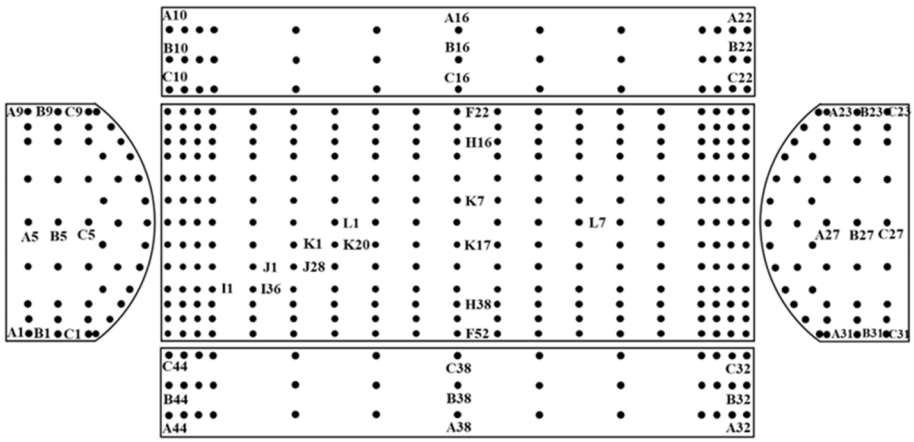

(a) Vaulted-roof model

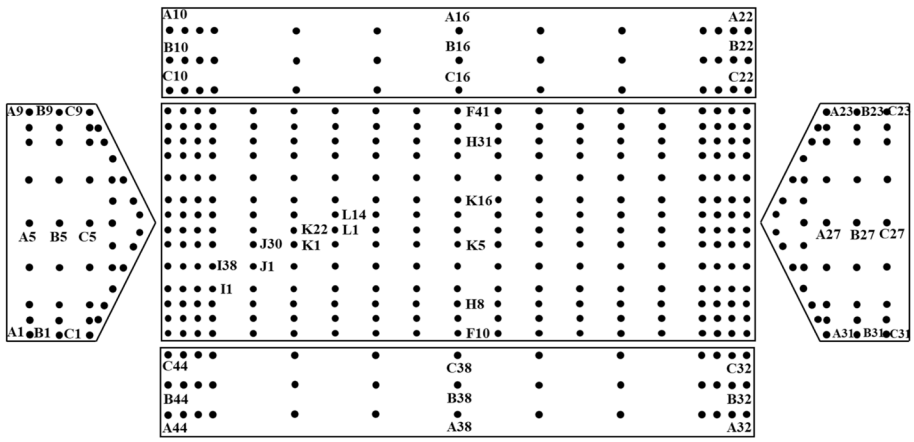

(b) Pitched-roof model

Fig. 2 Pressure tap distribution of the test models

the prototype [14], the 18 pieces of meridional rough paper tapes with a width of 8 mm and a thickness of 0.3 mm are pasted to the external surface of the model to compensate for Reynold number differences [15]. The arrangement of meridional paper tapes for the vaulted-roof model is shown in Fig. 3.

2.2 Simulation of the wind field in the wind tunnel

Rigid model pressure measurement experiments for the agricultural greenhouse buildings are conducted in the HD-3 straight-flow wind tunnel at Hunan University, China. The testing section of the wind tunnel is 10 m long, 3 m wide and 2.5 m high. The experiment speed can vary continuously from 0.5 m/s to 20 m/s. A turntable with a 1.8 m diameter is installed in the testing section to simulate the changing wind directions [16]. According to the measured results obtained by Huang et al. [17], the agricultural greenhouse building base on tropical islands roughly conforms to the Class B landform in the Load Code for the Design of Building Structures (GB 50009–2012) [18]. Passive simulation methods including spires, gratings, rough elements and baffles are utilized to generate the profiles of Class B in Chinese standard. The wind pressure signals are measured

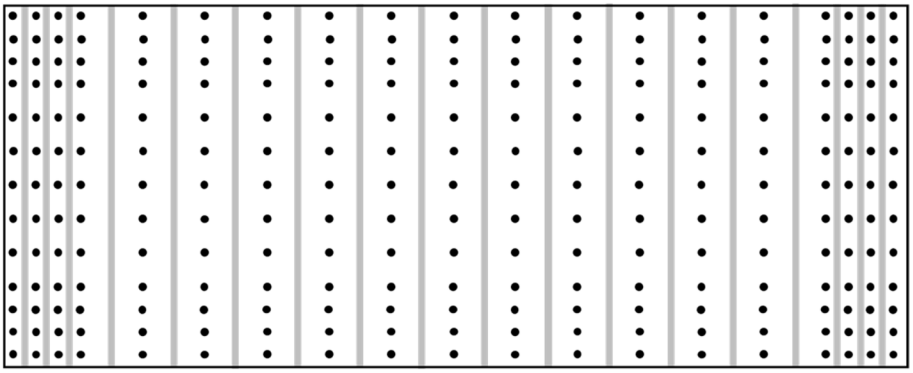

Fig. 3 Arrangement of meridional paper tapes for the vaulted roof

simultaneously at a sampling frequency of 312.5 Hz. The duration of sampling is 32 s and 10,000 data are collected at each measurement tap. The wind tunnel sampling time corresponds to the actual sampling time of 13.3 min, which meets the sampling time of not less than 10 min in the Chinese standard (GB 5009–2012). The reference height is 40 cm in the wind tunnel, which corresponds to the actual height of 10 m. The test wind speed is 10 m/s. Figure 4 shows the flow field simulation in the wind tunnel. In Fig. 4b and c, Z and Z_r represent the height of the wind speed sampling point and the reference height respectively, in m. U_z and U_r represent the wind speed at the height of Z and the wind speed at the reference height respectively, in m/s. I_u represents the turbulence intensity along the wind. The vertical coordinate $fS_u/\sigma^2{}_u$ represents the normalized wind speed spectrum value and the horizontal coordinate fL_u/U_r represents the reduce frequency, where f is the frequency of fluctuating wind, in Hz, σ_u is the standard deviation of the wind speed, and L_u is the turbulence integration scale at the reference height, in m. The results show that the wind speed profile, turbulence intensities, and wind speed spectrum simulated by the wind tunnel are consistent with the target values.

3 Results and discussions

3.1 Mean wind pressure coefficient

Four typical wind directions of 0°, 30°, 60° and 90° are mainly discussed because of the biaxial symmetry of the models. Figures 5 and 6 show the mean pressure coefficient contour on the vaulted roof and pitched roof, respectively. At the wind direction of 0°, the mean wind pressure coefficient contour is symmetrical on the vaulted roof due to the influence of the columnar vortex. Large pressure gradients are observed on the windward roof, while small pressure gradients appear on the leeward roof. The positive wind pressure coefficients occur in the zone near the eave and then decrease rapidly to negative pressure with the increasing distance from the windward eave. Finally, the mean pressure coefficients come to a minimum in the ridge. When the wind blows in oblique directions from 30° to 60°, the negative high-pressure zone gradually develops from the edge of the west gable to the windward eaves. At the wind direction of 90°, the negative pressure appears in the vast majority of areas on the roof. At the same time, the west gable transforms into the windward side, and the absolute value of the wind pressure

(a) Layout of the wind tunnel test

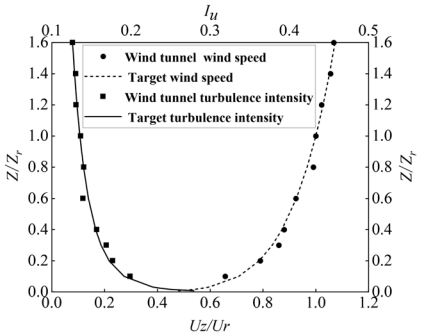

(b) Wind profiles and turbulence intensities of the flow field

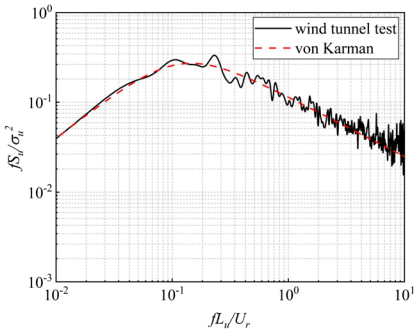

(c) Wind speed spectra at the reference height

Fig. 4 The flow field simulation in the wind tunnel

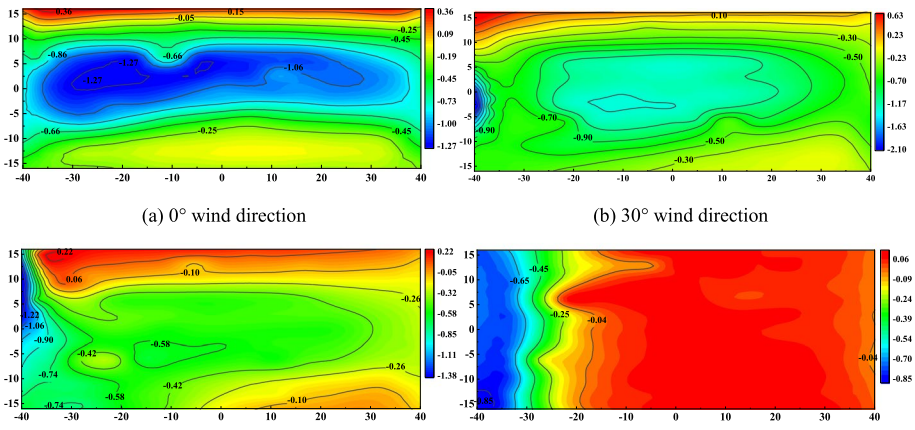

(a) 0° wind direction

(b) 30° wind direction

(c) 60° wind direction

(d) 90° wind direction

Fig. 5 The mean wind pressure coefficient distribution on the vaulted roof

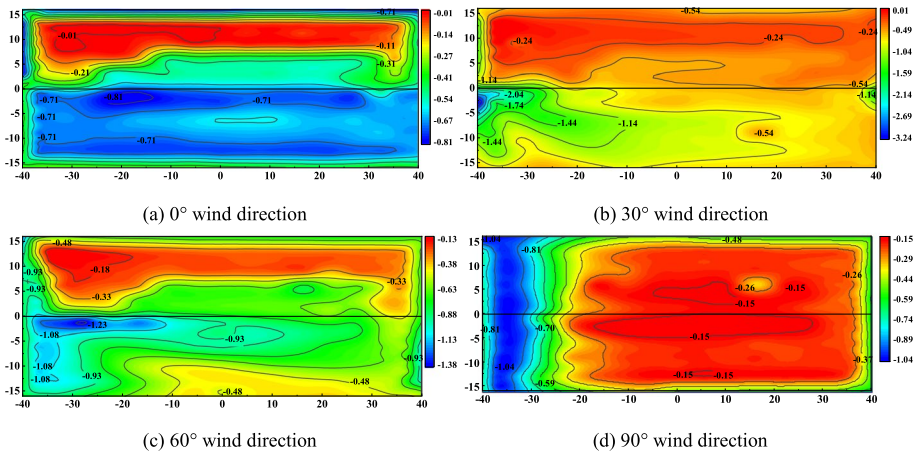

Fig. 6 The mean wind pressure coefficient distribution on the pitched roof

coefficient decreases rapidly with the increasing distance from the windward edge until it is near zero at 1/3 of the length of the roof.

The mean pressure coefficient distribution of the pitched roof is similar to that of the vaulted roof at the wind direction of 0°. Unlike a vaulted roof, the incoming flow is separated at the windward eave of the pitched roof so that the negative pressure appears in the windward eave and ridge, and the wind pressure in the middle of the windward roof is close to zero. When the wind blows in oblique directions from 30° to 60°, the negative high-pressure zone moves to the leeward area near the west gable and ridge. It is because the gable size of the windward edge is small, which is beneficial to the rapid entrainment and development of the separation shear layer. Besides, the ridge prevents the conical vortex from moving forward, and the downwind momentum of the conical vortex transforms into crosswind vorticity, so strong suction induced by the vortex develops along the ridge. At the wind direction of 90°, there are prominent negative pressures near the edge of the west gable because of the direct impact of the incoming flow. The absolute value of the wind pressure coefficient of the pitched roof is greater than that of the vaulted roof, and it gradually decreases along the ridge line, showing a symmetrical distribution.

When the wind directions are 0° and 90°, the mean wind pressure coefficients along the two buildings' midline are presented to deeply analyze the influence of roof shape on the mean wind pressure of agricultural greenhouse buildings. As shown in Fig. 7, the horizontal coordinate presents the ratio of the horizontal distance of the measuring tap to the windward eave to the building's span B or length L (the distance in the wall is after the planar unfolding), and the vertical coordinate represents the mean wind pressure coefficient. At the wind direction of 0°, the mean wind pressure coefficients present the same distribution pattern at the windward walls of two greenhouses and both reach the maximum at the second row B16 (near the 2/3 height of the windward wall). The wind pressure coefficient shows a "decrease first, then increase" on the vaulted roof, while a "monotonically decrease" on the pitched roof. The start and end points of the curves nearly coincide with the roof airflow separation and reattachment points, respectively. Compared with the pitched roof, larger negative pressure appears in the vaulted

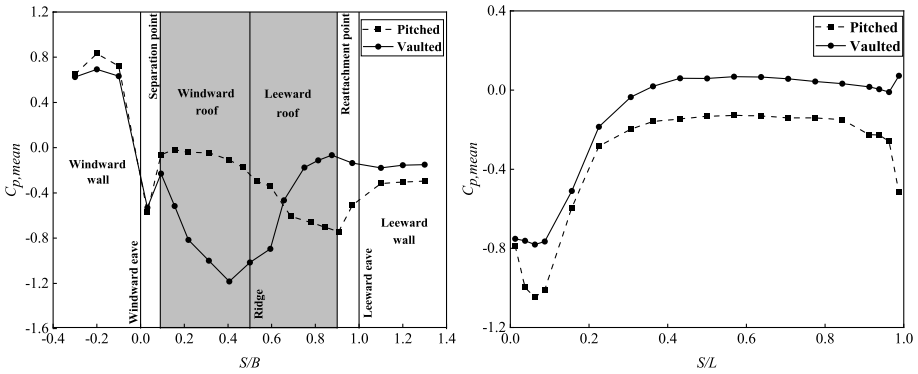

(a) 0° wind direction (b) 90° wind direction

Fig. 7 The mean wind pressure coefficients in the roof midline of the two greenhouses

windward roof. As for the leeward roof, the absolute value of the mean pressure coefficient of the vaulted roof decreases slowly and reaches 0 near the leeward eave, while that of the pitched roof gradually increases and reaches a maximum value of 0.75. At the wind direction of 90°, the mean pressure coefficients for the two greenhouses present a similar tendency with decreasing first, then increasing fast, and lastly tending to be uniform. The minimum of the vaulted roof and pitched roof is −0.79 and −1.05, respectively. When the airflow flows over 0.4 L along the length direction, the mean pressure coefficients of the vaulted roof are near 0. The mean pressure coefficients of the pitched roof are significantly less than 0. The absolute values of the mean pressure coefficients of the pitched roof are higher than those of the vaulted roof, which indicates the mean wind pressure is more sensitive to the pitched roof than the vaulted roof.

3.2 Fluctuating wind pressure coefficient

Figures 8 and 9 show the fluctuating pressure coefficient contour on the vaulted roof and pitched roof, respectively. When the wind direction is 0°, the fluctuating wind pressure coefficient contour is symmetrical on the vaulted roof. Two symmetrical high-pressure zones occur on the leeward roof near the gable verge, causing the gable to be easily

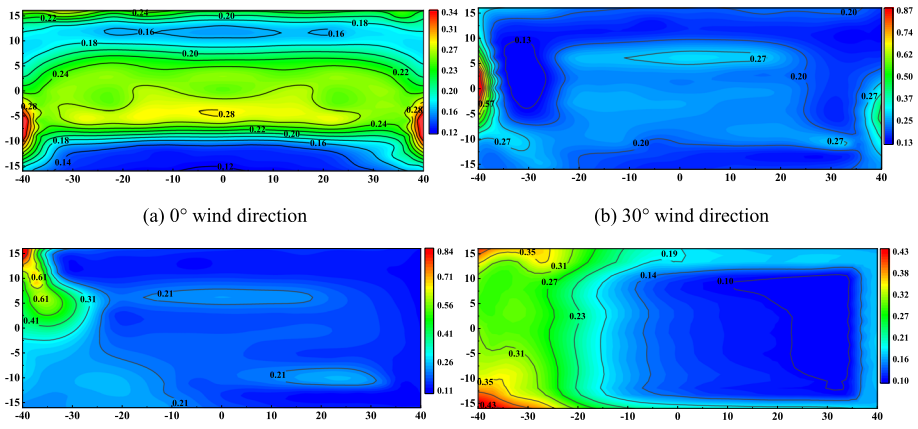

(a) 0° wind direction (b) 30° wind direction

(c) 60° wind direction (d) 90° wind direction

Fig. 8 The fluctuating wind pressure coefficient distribution on the vaulted roof

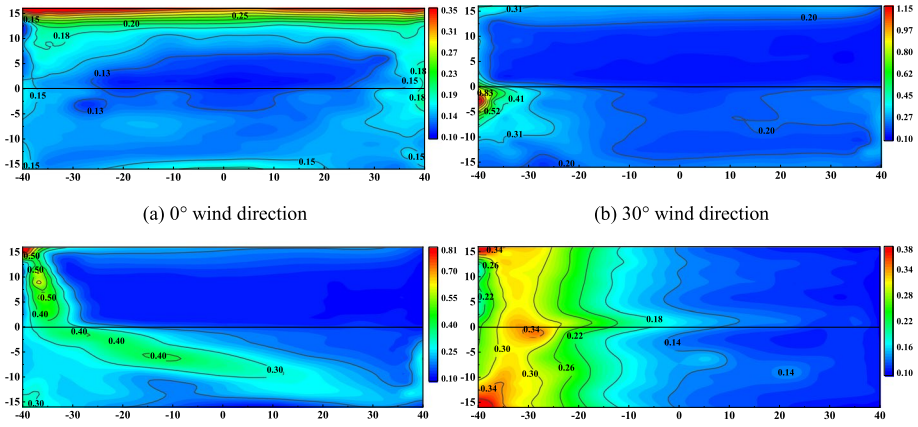

(a) 0° wind direction (b) 30° wind direction

(c) 60° wind direction (d) 90° wind direction

Fig. 9 The fluctuating wind pressure coefficient distribution on the pitched roof

damaged. When the wind blows in oblique directions from 30° to 60°, the contour distribution has similar characteristics, and the fluctuating wind pressure coefficients in most zones are small, about 0.20. Owing to the airflow separation in the corner, large gradients of the fluctuating wind pressure occur in the west gable near the windward zone. At the wind direction of 90°, the high wind pressure zone occurs in the windward corner near the west gable. The fluctuating wind pressure coefficient decreases rapidly with the increasing distance from the windward gable. Similar to the distribution of the mean wind pressure coefficient, the fluctuating wind pressure coefficient tends to flatten after crossing 1/3 of the length of the roof.

When the wind direction is 0°, as for the pitched roof, the fluctuating wind pressure coefficient reaches the maximum in the windward eave and then decreases towards the ridge direction. The fluctuating wind pressure changes slowly on the leeward roof. When the wind blows in oblique directions from 30° to 60°, the high-pressure zones move from the middle zones of the west gable and the windward corner to the leeward eave, and a high-pressure ribbon is observed on the pitched roof, which deserves to be emphasized in the design of greenhouse buildings. At the wind direction of 90°, similar to the distribution of fluctuating wind pressure coefficients for the vaulted roof, high fluctuating pressure coefficients appear in the windward front zone of the gable and then come to flatten as airflow develops.

Similar to Fig. 7, to analyze the influence of roof shape on the fluctuating wind pressure of agricultural greenhouse buildings, Fig. 10 shows the fluctuating wind pressure coefficients along the two buildings' midlines at the wind directions of 0° and 90°. When the wind direction is 0°, the fluctuating wind pressure coefficients present a similar distribution pattern at the windward walls of the two greenhouses, and the fluctuating wind pressure coefficients of the pitched model are slightly higher than those of the vaulted model. Between the airflow separation point and reattachment point on the roof, the fluctuating wind pressure coefficients of the vaulted roof show an "increase first, then decrease", while those of the pitched roof show a "decrease first, then increase slowly". The inflection points of the two curves are near the ridge, which presents different distribution patterns from the mean wind pressure coefficient. At the same time, the wind

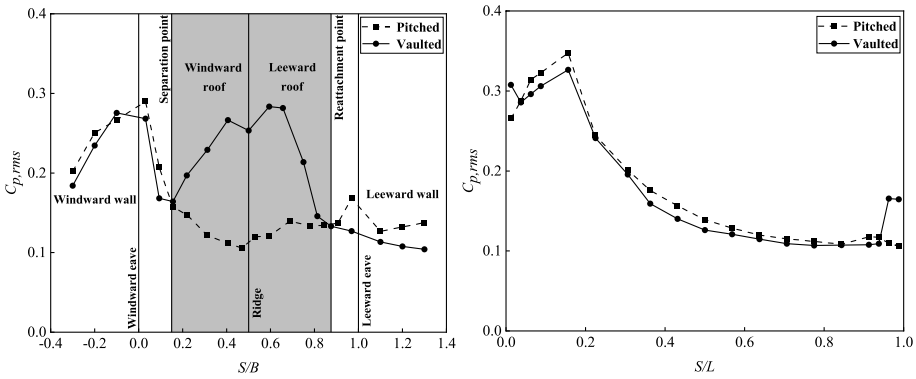

(a) 0° wind direction (b) 90° wind direction

Fig. 10 Comparison of the fluctuating pressure coefficients in the roof midline of the two greenhouses

pressure fluctuation of the vaulted roof is more significant than that of the pitched roof. It is because the incoming flow is separated locally in the lateral region of the vaulted roof, resulting in a transverse separation shear flow, which forms the vortex shedding in the roof fluid and produces high turbulent kinetic energy [19]. In addition, the distribution of fluctuating wind pressure on the vaulted roof is significantly affected by the Reynolds number, and the flow transition near the airflow separation point leads to high fluctuating wind pressure [14]. When the wind direction is 90°, the fluctuating pressure coefficients for two greenhouses present a similar tendency with increasing first, then decreasing slowly, and lastly tending to be uniform. The fluctuating pressure coefficients of the pitched roof are slightly higher than those of the vaulted roof, which indicates the fluctuating pressure coefficients are more sensitive to the pitched roof than the vaulted roof.

3.3 Wind load shape coefficient

Different countries' standards have corresponding provisions in determining wind load shape coefficients for agricultural greenhouse buildings with different roof shapes. The surface of the vaulted-roof model is divided into several matching zones so that the results for the wind tunnel test can be compared with four countries' standards: China, Japan, the U.S., and the European Union (EU) [20–23]. Surface zone definitions of the vaulted-roof model are shown in Fig. 11a, b, c and d. As for the pitched-roof model, the four countries' standards have the same surface zones. Surface zone definitions of the pitched-roof model are shown in Fig. 11e.

Table 1 shows the comparative results of the wind load shape coefficient between the experiment and four countries' standards and references for the vaulted-roof greenhouse. The standards from China and Japan have the same surface zone definitions for the vaulted-roof greenhouse and are defined as "Comparison 1" group. Surface zone definitions from Kwon [4] and Blackmore [24] are close to the standard from the EU, so they are defined as "Comparison 3" group. Surface zone definitions from the American standard differ from the above standards and references, so the experiment results are compared separately with the American standard as a "Comparison 2" group.

Combined with Tables 1 and 2, the experiment values in the R1 region are in good agreement with Blackmore's results, with a small deviation of 25.4% from the Japanese

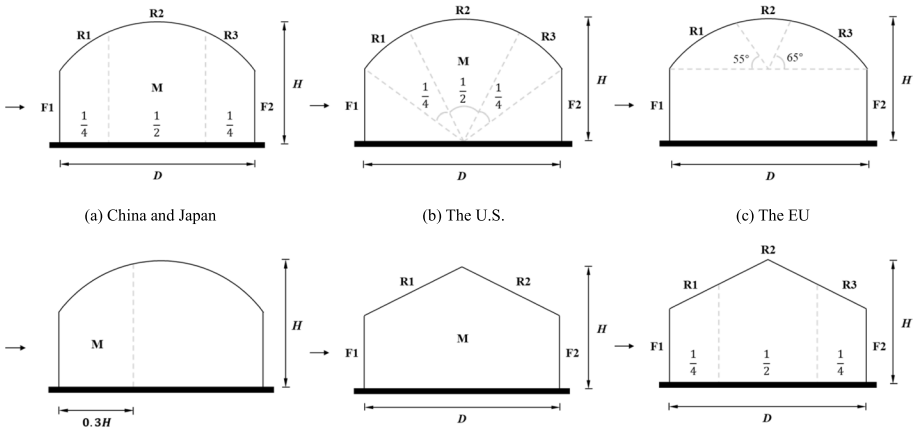

(a) China and Japan (b) The U.S. (c) The EU

(d) The gable zone definitions for the EU (e) Surface zone definitions for four countries (f) Surface zone definitions for the comparison

Fig. 11 Surface zone definitions of the vaulted-roof and the pitched-roof greenhouses

Table 1 Wind load shape coefficients for the vaulted-roof greenhouse

Zone definitions	Comparison 1			Comparison 2		Comparison 3			
	Result 1	China	Japan	Result 2	The U.S.	Result 3	The EU	Kwon [4]	Blackmore [24]
R1	−0.47	+0.10	−0.63	−0.34	+0.08	−0.37	+0.30	−0.64	−0.36
R2	−1.08	−0.80	−1.32	−0.80	−0.95	−0.97	−1.00	−1.35	−0.41
R3	−0.43	−0.50	−0.50	−0.30	−0.50	−0.39	−0.40	−0.85	−0.42
F1	+0.83	+0.80	+0.60	+0.83	+0.80	+0.83	+0.60	+0.52	—
F2	−0.49	−0.50	−0.50	−0.49	−0.50	−0.49	−0.41	−0.64	—
M	−0.68	−0.70	−0.57	−0.68	−0.70	−0.88	−1.00	−0.97	—

Table 2 Deviations of test results from existing standards and references for the vaulted-roof greenhouse

Zone definitions	China	Japan	The U.S.	The EU	Kwon	Blackmore
R1	570.0%	25.4%	525.0%	223.3%	42.2%	2.8%
R2	35.0%	18.2%	15.8%	3.0%	28.1%	136.6%
R3	14.0%	14.0%	40.0%	2.5%	54.1%	7.1%
F1	3.8%	38.3%	3.8%	38.3%	59.6%	—
F2	2.0%	2.0%	2.0%	19.5%	23.4%	—
M	2.9%	19.3%	2.9%	12.0%	9.3%	—
Average	104.6%	19.5%	98.3%	49.8%	36.1%	48.8%

standard and increasing deviations from the EU, U.S., and Chinese standards in that order. The standards of the four countries pay different attention to the geometrical characteristics of greenhouse buildings, which leads to the deviation of the shape coefficient. Regarding the determination of shape coefficients, the Japanese standard is the most detailed in describing the shape coefficients, and involves the main geometrical characteristics of the experimental model, so the deviation between the experiment results and the Japanese standard is the smallest. The rest of the standards reflect partly the geometrical characteristics of the experimental model, so the experiment results

deviate significantly from the standards. It should be clarified that although the standards from China and Japan have the same surface zone definitions, the Chinese standard only reflects the effect of the rise-to-span ratio on wind loads, while the Japanese standard comprehensively reflects the effect of the rise-to-span ratio and eave height-to-span ratio on wind loads, where the shape coefficient in the R1 zone increases with increasing windward length [23]. The deviations from references may be due to the differences in the geometrical characteristics and Reynolds numbers [14, 25, 26].

The experiment values in the R2 and R3 regions are in good agreement with the standard from the EU. The experiment value in the R2 region shows the largest deviation from Blackmore's results at 136.6% and the experiment value in the R3 region shows the largest deviation from Kwon's results at 54.1%. The experiment value in the F1 region matches the standards from China and the U.S., is larger than the standards from Japan and the EU, and has the largest deviation from Kwon's result at 59.6%. The experiment value in the F2 region matches the standards from China, the U.S. and Japan, with the largest deviation from Kwon's result at 23.4%. The experiment value in the M region is in agreement with the standards from China and the U.S., with deviations of 9.3%, 12.0% and 19.3% from Kwon's results, the standards from the EU and Japan, respectively. In summary, the shape coefficient experiment result of the vaulted-roof greenhouse shows the smallest deviation from the Japanese standard, with an average deviation of 19.5% for all surface zones, and shows the largest deviation from the Chinese standard, with an average deviation of 104.6%. In conclusion, the results indicate that the standards from China, Japan, the U.S., and the EU all have limitations in determining the wind load shape coefficient for the vaulted-roof greenhouse.

Table 3 shows the comparative results of the wind load shape coefficient between the experiment and four countries' standards and references for the pitched-roof greenhouse. The standards of the four countries pay different attention to the geometrical parameters of greenhouse buildings, which leads to differences in the shape coefficients of greenhouse buildings with the same dimension. The standard from China is only related to the slope angle, and the standards from the U.S. and the EU comprehensively reflect the effect of the slope angle and height-to-width ratio on wind loads. The standard from Japan reflects the combined effect of the slope angle, length-to-height ratio and width-to-height ratio to meet the requirements of its country. Combined with Tables 3 and 4, the experiment value in the R1 region has the smallest deviation from the standards from the U.S. and the EU at 25.9%, and the largest deviation from Kwon's result

Table 3 Wind load shape coefficients for the pitched-roof greenhouse

Zone Definitions	Experiment	China	The U.S.	The EU	Japan	Wells [2]	Kwon [4]
R1	−0.20	−0.14	−0.27	−0.27	−0.14	0.00	−0.77
R2	−0.60	−0.50	−0.60	−0.67	−0.60	−0.57	−0.71
F1	+0.80	+0.80	+0.80	+0.66	+0.60	+0.60	+0.57
F2	−0.50	−0.50	−0.50	−0.36	−0.50	−0.60	−0.16
M	−0.64 (−1.1)	−0.70	−0.70	−1.0	−0.70	−0.60	−0.71

The value in the bracket refers to the experiment value matching the zone definitions of the gable from the standard from the EU

Table 4 Deviations of test results from existing standards and references for the pitched-roof greenhouse

Zone Definitions	China	The U.S.	The EU	Japan	Wells	Kwon
R1	42.9%	25.9%	25.9%	42.9%	—	74.0%
R2	20.0%	0.0%	10.4%	0.0%	5.0%	15.5%
F1	0.0%	0.0%	21.2%	33.3%	25.0%	40.4%
F2	0.0%	0.0%	38.9%	0.0%	20.0%	212.5%
M	8.6%	8.6%	10.0%	8.6%	6.7%	9.9%
Average	14.3%	6.9%	21.3%	17.0%	14.2%	70.4%

Table 5 Comparison of the wind load shape coefficients in the same zones of the two greenhouses

Roof shape	R1	R2	R3
Vaulted roof	−0.47	−1.08	−0.43
Pitched roof	−0.18	−0.29	−0.62

at 74.0%. The experiment value in the R2 region matches the American and Japanese standards as well as Wells' results, with the largest deviation from the Chinese standard at 20.0%. The experiment value in the F1 region matches the Chinese and American standards, and is greater than the standards from the EU and Japan as well as Wells' and Kwon's results, with the greatest deviation from Kwon's results at 40.4%. The standard from Japan has the most detailed description of the F1 region among the four countries' standards, which reflects the influence of the variation coefficient along the height direction. The experiment value in the F2 region matches the standards from China, the U.S. and Japan, with the largest deviation from Kwon's result at 212.5%. The experiment value in the M region shows small deviations from the four countries' standards and references, with the largest deviation occurring in the standard from the EU at 10.0%. In summary, the shape coefficient experiment result of the pitched-roof greenhouse has the smallest average deviation of all zones from the American standard, at 6.9%, and has the greatest average deviation from Kwon's result, at 70.4%. In conclusion, the results indicate that the American standard can basically describe the shape coefficients of the pitched-roof greenhouse, while the rest of standards have limitations in determining the shape coefficients of the pitched-roof greenhouse.

To further analyze the influence of roof shape on the shape coefficient, as shown in Fig. 11f, the pitched roof greenhouse is divided into several matching zones with the vaulted roof greenhouse in Chinese and Japanese standards. Table 5 shows that the roof shape has a significant influence on the distribution of the shape coefficients. Compared with the pitched roof, the R1 region in the windward front zone and the R2 region in the middle roof show higher negative pressure in magnitude for the vaulted roof, with a deviation of 161.1% and 272.4%, respectively. The absolute value of the shape coefficient in the R3 region on the vaulted leeward roof is smaller than that on the pitched leeward roof. The results demonstrate that the vaulted roof shape will increase the suction effect on the windward front zone and the middle roof while mitigating the suction effect on the leeward roof.

3.4 Wind-pressure non-Gaussian characteristics

Influenced by flow separation, reattachment and vortex shedding, the wind-pressure signals collected in the local zone present significant non-Gaussian characteristics. As for the low-rise buildings, Kumar [27] considers the zone with the absolute skewness $|S_K| > 0.5$ and kurtosis $C_K > 3.5$ as the wind-pressure non-Gaussian zone. Agricultural greenhouses are significantly different from general low-rise buildings, so this criterion does not apply to the determination of the non-Gaussian characteristics of wind pressure on greenhouses. Additionally, at the same measuring tap, whether the fluctuating wind load conforms to a Gaussian distribution is closely related to the incoming wind direction [28]. Therefore, the concept of statistical cumulative probability is introduced in this study to explore the cumulative probability of different wind directions, and further strengthen the Gaussian-non-Gaussian basis for the classification of skewness and kurtosis. Previous studies have demonstrated that reaching a cumulative probability of 80% serves as a critical point for defining the cumulative distribution of long-span flat roof and cylindrical roof cover skewness and kurtosis as a high-probability event [28–32]. The vaulted and pitched roofs in this study also belong to the above-mentioned long-span roofs. Since the study object is similar to the appearance of the long-span roof, the values of the skewness coefficients and kurtosis coefficients corresponding to 80% cumulative probability are selected as the critical points, and then the values are regarded as the criteria of wind-pressure non-Gaussian characteristics.

Figure 12 shows the cumulative probability distribution curves of skewness and kurtosis for the vaulted-roof and pitched-roof greenhouses at the wind direction of 0°, from which the critical values at each wind direction are further obtained by 80% cumulative probability. It is observed in Table 6 that the critical values of skewness and kurtosis at wind directions from 15° to 75° are close to each other, so the approximate mean values of the skewness and kurtosis coefficients at wind directions from 15° to 75° are taken as the determination criterion at the oblique wind directions. In this study, the wind-pressure measurement taps with $|S_K| \leq S$ and $C_K \leq C$ are regarded as Gaussian points, and the taps with $|S_K| > S$ and $C_K > C$ are regarded as non-Gaussian points, then the rest of the wind-pressure taps with $|S_K| < S$ and $C_K > C$ or $|S_K| > S$ and $C_K < C$ are further systematically judged according to the combination with the wind-pressure time-history curve and the probability histogram. The F9 measuring tap (failure to meet the direct determination criterion in Table 6) near the gable verge of the vaulted-roof greenhouse at the wind direction of 0° is selected as an example to introduce the judgment procedure. The wind-pressure time-history curve and the probability histogram of F9 are illustrated in Fig. 13. The results show that the wind-pressure time-history curve presents an asymmetry and the intermittent pulse phenomenon and diverges from the Gaussian

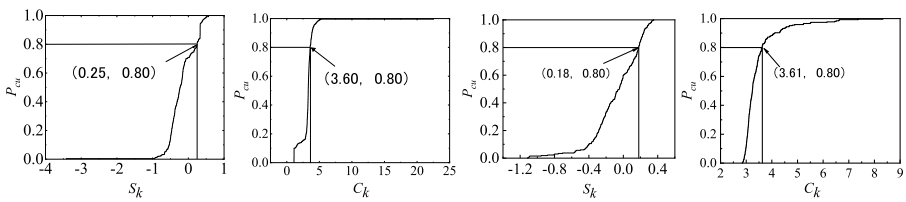

(a) Skewness of vaulted roof (b) Kurtosis of vaulted roof (c) Skewness of pitched roof (d) Kurtosis of pitched roof

Fig. 12 The cumulative probability distribution curves of skewness and kurtosis at the wind direction of 0°

Table 6 The determination criterion of wind-pressure non-Gaussian characteristics of the two greenhouses

Wind direction	Vaulted roof		Pitched roof	
	The critical skewness coefficient *S*	The critical kurtosis coefficient *C*	The critical skewness coefficient *S*	The critical kurtosis coefficient *C*
0°	0.25	3.60	0.18	3.61
15°	0.08	3.84	0.12	4.24
30°	0.06	3.87	0.08	4.21
45°	0.07	3.81	0.09	4.16
60°	0.10	3.75	0.11	4.20
75°	0.07	3.90	0.10	4.20
(15°–75°)	(0.08)	(3.83)	(0.10)	(4.20)
90°	0.04	4.21	0.18	4.04

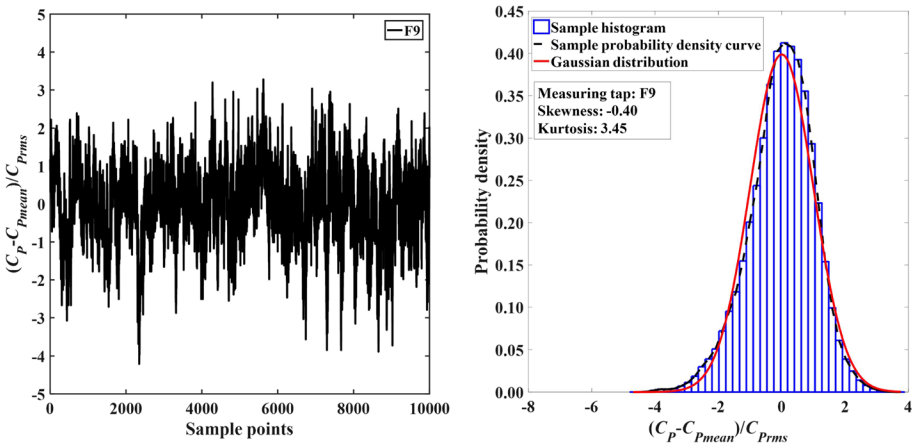

(a) The wind-pressure time-history (b) The probability histogram

Fig. 13 The wind-pressure time-history and probability histogram of measuring tap F9 on the vaulted roof at 0°

distribution curve, which indicates the F9 measuring tap does not follow the Gaussian distribution. Non-Gaussian characteristics of the measuring taps on the two greenhouse roofs are analyzed according to the determination criteria or the time-history curve and probability histogram. Figures 14 and 15 show the Gaussian and non-Gaussian distribution of wind pressure on the vaulted roof and pitched roof, respectively, among which the shadow area shows the Gaussian distribution and the rest of the areas show the non-Gaussian distribution.

As shown in Fig. 14, influenced by the signature turbulence, the vaulted roof presents the following characteristics: (1) At the wind direction of 0°, the non-Gaussian zone appears in the windward eave and the leeward eave. The former is caused by the separation of the incoming flow in the windward eaves, and the latter is attributed to the disturbance and mutual interference of wake wind pressure caused by the reattachment of the separated flow in the leeward eaves. (2) When the wind blows in oblique directions from 15° to 75°, non-Gaussian zones appear in the edge, corner,

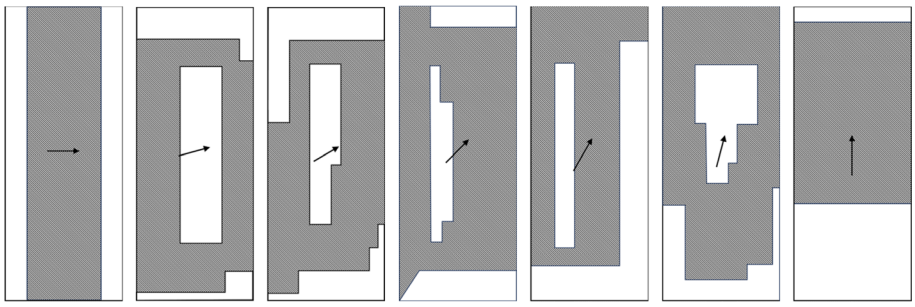

(a) $\alpha = 0°$ (b) $\alpha = 15°$ (c) $\alpha = 30°$ (d) $\alpha = 45°$ (e) $\alpha = 60°$ (f) $\alpha = 75°$ (g) $\alpha = 90°$

Fig. 14 Wind-pressure non-Gaussian zones of the vaulted roof at different wind directions

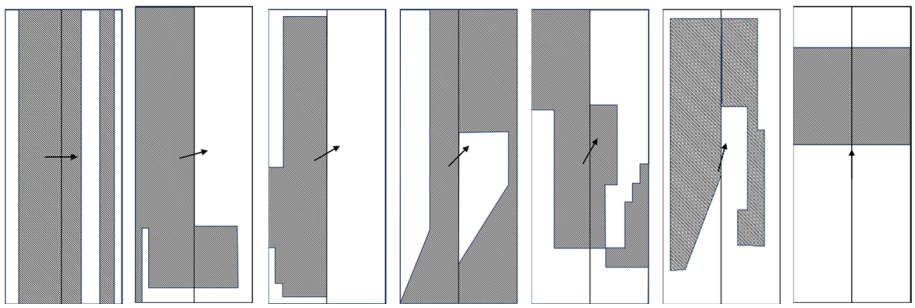

(a) $\alpha = 0°$ (b) $\alpha = 15°$ (c) $\alpha = 30°$ (d) $\alpha = 45°$ (e) $\alpha = 60°$ (f) $\alpha = 75°$ (g) $\alpha = 90°$

Fig. 15 Wind-pressure non-Gaussian zones of the pitched roof at different wind directions

and roof middle zones. With increasing wind directions, the wind-pressure non-Gaussian area in the windward gable enlarges, and that in the leeward verge declines, which is attributed to the separation flow in the shear layer, the side-to-side oscillatory motion of the conical vortex axis, and the secondary vortex [33]. (3) At the wind direction of 90°, the symmetrical non-Gaussian zones appear in the windward front zone and leeward verge zone. In general terms, as for the vaulted roof, wind-pressure non-Gaussian areas are mainly distributed in the windward front zone, the leeward back zone and the roof middle zone.

As shown in Fig. 15, the pitched roof presents the following characteristics: (1) When the wind direction is 0°, wind-pressure non-Gaussian zones appear in the windward front area and the middle and verge area of the leeward roof. That is because the incoming flow separates and reattaches when the airflow flows over the windward eave and ridge. (2) When the wind blows in oblique directions from 15° to 75°, influenced by the flow separation, a pair of conical vortexes appears in the corner and the ridge, which leads to the wind-pressure non-Gaussian characteristics in the windward front zone and the localized zone of the leeward roof. Besides, the non-Gaussian area in the windward edge and corner increases with increasing wind directions. Especially, a non-Gaussian ribbon is observed on the leeward roof at the wind direction of 60°, which is the same as the fluctuating wind pressure distribution. (3) At the wind direction of 90°, the symmetrical non-Gaussian distribution zones are observed in the windward front zone and leeward back zone. In conclusion, as for the pitched roof, the wind-pressure non-Gaussian zones are mainly distributed in the windward front zone and the leeward roof.

The windward front zones of the vaulted roof and the pitched roof all show non-Gaussian characteristics. The difference is that the wind pressure distribution in the middle roof of the vaulted greenhouse is non-Gaussian, while that in the leeward roof of the pitched greenhouse is non-Gaussian. In a word, compared with the vaulted roof, the pitched roof presents more obvious wind-pressure non-Gaussian characteristics at each wind direction.

3.5 Wind pressure spectrum

The fluctuating wind pressure spectrum is a diagram that not only can depict the wind pressure signal distribution in the frequency domain, but also directly reflects the magnitude of the signal carrying power per unit frequency band. The wind pressure fluctuation on the roof includes the low-frequency and the high-frequency components. The low-frequency component comes from the large-scale turbulent structure in the incoming flow, and the high-frequency component comes from the small-scale turbulent structure closed to the solid wall, which is caused by the disturbing effect of the structure itself on the incoming flow [33]. Hence, the wind pressure spectrum not only displays the contribution of the wind pressure signal to the fluctuating wind pressure in different frequency components, but also identifies the potential turbulent structure [34]. In this study, the wind pressure spectra at the same measuring taps located on the surface of the vaulted-roof and pitched-roof greenhouses at the wind direction of 0° are presented. To obtain accurate wind pressure data, the Butterworth filter is adopted to eliminate the noise influence of the electrical signals in the test system [34–36]. As shown in Fig. 16, the horizontal coordinate fB/U_z represents the reduced frequency, and the vertical coordinate fS_p/σ^2_p represents the normalized wind pressure spectrum values.

The results show that at the number 1 measuring tap, the wind pressure spectra of the vaulted-roof and pitched-roof greenhouses have a similar trend, and the corresponding peak frequencies are all close to 1. However, as the distance between the measuring tap and the windward eave increases, the peak frequency of the pitched-roof greenhouse shows a gradually increasing movement. At the number 3 measuring tap of the vaulted-roof greenhouse, it is also found that the faster energy decay occurs in the high-frequency components.

Figure 16a depicts the wind pressure spectra at measuring taps on the windward roof. It is observed that the normalized wind pressure spectrum value of the vaulted-roof model is higher than that of the pitched-roof model in the low-frequency components. However, with the development of airflow (the measuring taps change from 1 to 3), the misalignment between the two curves gradually expands. In the high-frequency components, the wind pressure spectrum value of the pitched-roof model is higher than that of the vaulted-roof model. It may be because small-scale turbulence generates some vortices after the airflow separation in the shear layer of the pitched-roof model.

Figure 16b depicts the wind pressure spectra at measuring taps on the leeward roof. The wind pressure spectrum at the number 4 measuring tap has a similar trend as the numbers 1 – 3. However, at the number 5 measuring tap, the wind pressure spectrum value of the vaulted-roof model is lower than that of the pitched-roof model in the low-frequency components, and the corresponding peak frequency of the leeward roof is higher than that of the windward roof for the vaulted-roof model. Besides, the

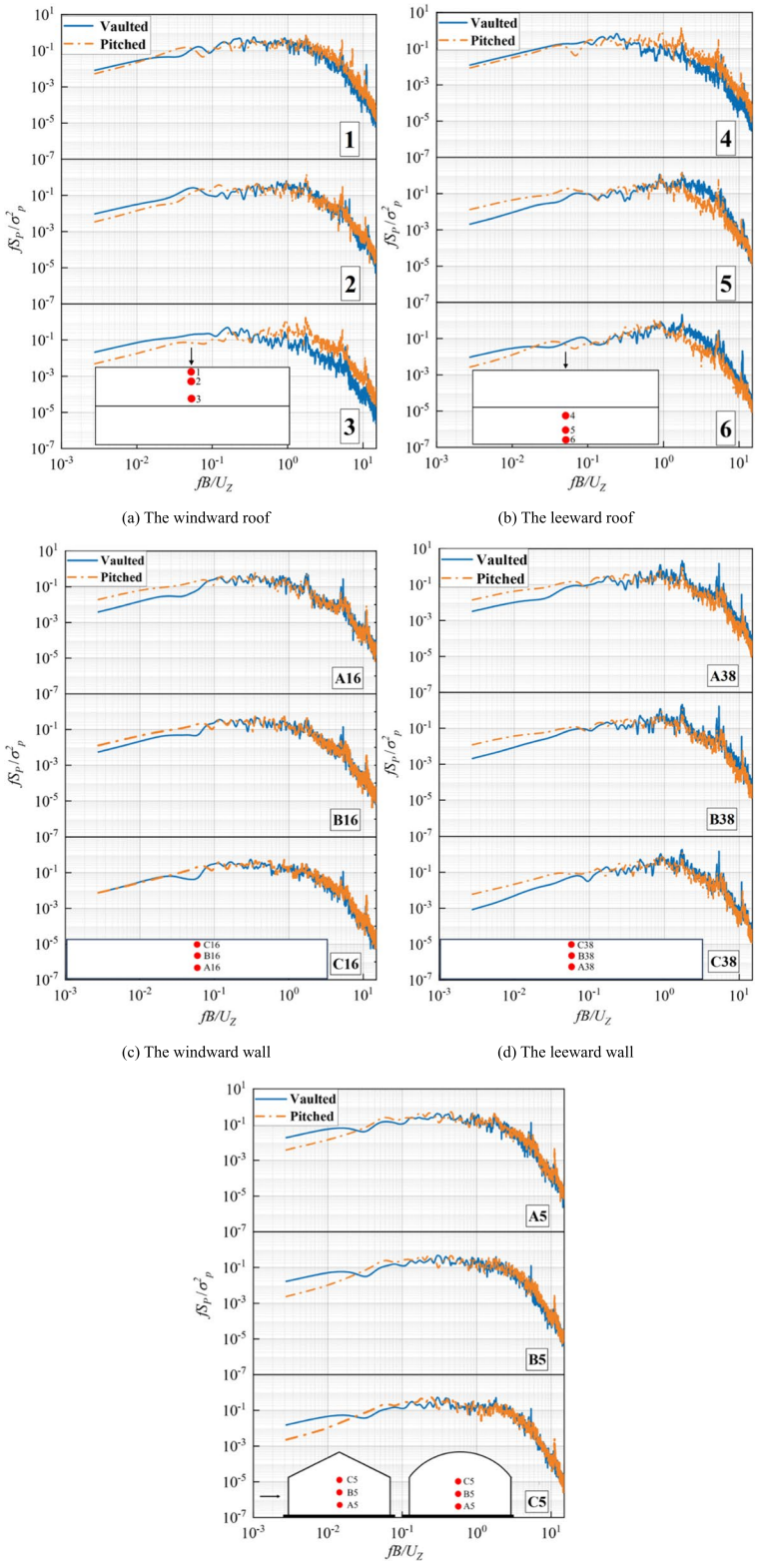

(a) The windward roof

(b) The leeward roof

(c) The windward wall

(d) The leeward wall

(e) The gable

Fig. 16 Comparison of wind pressure spectra of identical measuring taps for the two greenhouses at 0°

wind pressure spectrum value of the pitched-roof model decreases faster in the high-frequency components at the number 5 measuring tap. For both pitched and vaulted roofs, some pronounced peaks appear at specific frequencies, and this may be explained by the Helmholtz resonance phenomenon [37]. The Helmholtz resonance occurs inside the model cavity and the frequency corresponding to the pronounced peaks is the Helmholtz frequency.

Figure 16c, d and e depict the wind pressure spectra at measuring taps on walls. On the windward wall, the wind pressure spectrum value of the vaulted-roof model is lower than that of the pitched-roof model in the low-frequency components; besides, as the measuring tap height increases, the deviation is lower and lower. On the leeward wall, all of the wind pressure spectrum values of the vaulted-roof model are lower than those of the pitched-roof model in the low-frequency components. As for the gables, the wind pressure spectrum value of the vaulted-roof model is higher than that of the pitched-roof model in the low-frequency components. In conclusion, the energy distribution of the vaulted-roof and the pitched-roof models presents a similar trend in the middle-frequency and high-frequency components, which indicates the roof shape mainly affects the energy in the low-frequency components of the walls, while having little effect on the middle-frequency and high-frequency components of the walls.

4 Conclusion

In this study, wind pressure measurement tests of two typical agricultural greenhouse buildings were conducted in a wind tunnel, and the influence of the roof shape on the wind pressure characteristics was analyzed. The results provide a reference for the wind-resistant design of agricultural greenhouse buildings on tropical islands. The following conclusions can be drawn:

(1) The mean and fluctuating wind pressure distribution patterns and the localized high-pressure generation mechanism for the vaulted-roof and pitched-roof greenhouse buildings on tropical islands are clarified.
(2) The experimental shape coefficient of the pitched-roof greenhouse is basically consistent with the standard from the U.S., while that of the vaulted-roof greenhouse has some deviation from the existing standards. It is suggested that the experimental results should be used in the structural design. The vaulted roof shape will increase the suction effect on the windward front zone and the middle roof while mitigating the suction effect on the leeward roof.
(3) Wind pressure non-Gaussian determination criteria for agricultural greenhouse buildings considering the roof shape and wind directions are proposed. Compared with the vaulted roof, the pitched roof presents more obvious wind-pressure non-Gaussian characteristics at each wind direction.
(4) On the windward roof, the wind pressure spectrum value of the vaulted-roof model is higher than that of the pitched-roof in the low-frequency components, while slightly lower than that in the high-frequency components. In terms of the walls, the roof shape mainly affects the energy in the low-frequency components, while having little effect on the middle-frequency and high-frequency components.

Acknowledgements
We would like to thank all the experimental staff of the HD-3 Wind Tunnel for their hard work.

Authors' contributions
Bin Huang: Supervision, Methodology, Writing – original draft, Writing – review & editing, Funding acquisition. Jinke Liu: Methodology, Writing – original draft, Writing – review & editing. Zhengnong Li: Supervision, Conceptualization. Wenxiang Wang: Writing – review & editing, Software. Xiangjun Wang: Investigation, Writing – review & editing. Xijie Liu: Investigation, Software. Tianyin Xiao: Formal analysis.

Funding
This research was supported by the National Natural Science Foundation of China (52068019) and the Hainan Provincial Natural Science Foundation of China (522RC605, 520QN231 and 521RC502).

Availability of data and materials
The data that support the findings of this study are available from the corresponding author upon reasonable request.

Declarations

Competing interests
The authors declare that they have no competing interests.

Received: 11 October 2023 Accepted: 11 December 2023
Published online: 08 January 2024

References

1. Li H, Huang B, Liu J et al (2022) Review on wind resistance of thin-film greenhouse buildings in tropical islands. J Nat Disasters 31(05):13–23
2. Wells DA, Hoxey RP (1980) Measurements of wind loads on full-scale glasshouses. J Wind Eng Ind Aerodyn 6(1–2):139–167
3. Richardson GM (1986) Wind loads on a full-scale film-plastic clad greenhouse: with and without shelter from a windbreak. J Wind Eng Ind Aerodyn 23:321–331
4. Kwon K-S, Kim D-W, Kim R-W et al (2016) Evaluation of wind pressure coefficients of single-span greenhouses built on reclaimed coastal land using a large-sized wind tunnel. Biosyst Eng 141:58–81
5. Moriyama H, Sase S, Uematsu Y et al (2008) Wind pressure coefficient of a pipe-framed greenhouse and influence of the side gable openings using a wind tunnel. SASJ 38:237–248
6. Moriyama H, Sase S, Uematsu Y et al (2010) Wind tunnel study of the interaction of two or three side-by-side pipe-framed greenhouses on wind pressure coefficients. Trans ASABE 53(2):585–592
7. Kim R-W, Lee I-B, Yeo U-H et al (2019) Evaluation of various national greenhouse design standards for wind loading. Biosyst Eng 188:136–154
8. Kim R-W, Lee I-B, Kwon K-S et al (2017) Evaluation of wind pressure acting on multi-span greenhouses using CFD technique, part 1: development of the CFD model. Biosyst Eng 164:235–256
9. Yang ZQ, Li YX, Xue XP et al (2013) Wind loads on single-span plastic greenhouses and solar greenhouses. HortTechnology 23(5):622–628
10. Xie X, Chen K (2000) Simulation test of wind load characteristics of South China type single-span plastic greenhouse. Trans CSAE 16(5):90–94
11. Wu YF (2007) Research on load of greenhouse structure induced by wind force. Dissertation, Nanjing Agricultural University (in Chinese)
12. Surry D, Kopp GA, Bartlett FM (2005) Wind load testing of low buildings to failure at model and full scale. Nat Hazards Rev 6(3):121–128
13. Dong X, Ye JH, Ding JM (2018) Review of destructive vortices and vortex-induced wind pressures on low-rise buildings. J Build Struct 39(01):1–10
14. Sun Y, Qiu Y, Wu Y (2016) Research on effects of the geometric characteristics on critical Reynolds number ranges of cylindrical roofs in wind tunnel. J Build Struct 37(12):10–19
15 Zhao L, Ge Y, Kareem A (2017) Fluctuating wind pressure distribution around full-scale cooling towers. J Wind Eng Ind Aerodyn 165:34–45
16. Huang B (2019) Study on the flow field of wind-blown sand and its effect on low-rise buildings. Dissertation, Hunan University (in Chinese)
17. Huang B, Li H, Dong JS et al (2023) Wind profile in island areas by a wind measurement system of six-rotor UAV. J Hunan Univ Nat Sci 50(5):102–113 (in Chinese)
18. MOHURD (2012) Load code for the design of building structures, GB50009-2012. China Architecture Publishing & Media Co Ltd, Beijing
19. Toy N, Tahouri B (1988) Pressure distributions on semi-cylindrical structures of different geometrical cross-sections. J Wind Eng Ind Aerodyn 29(1–3):263–272
20. MOA (2016) Code for the design load of horticultural greenhouse structures, GB/T 51183-2016. China Planning Press, Beijing
21. ASCE (2016) Minimum design loads and associated criteria for buildings and other structures, ASCE/SEI 7-16. American Society of Civil Engineers, Reston

22. CEN (2019) Greenhouses - Design and construction - Part 1: Commercial production greenhouses, EVS-EN 13031-1:2019. European Committee for Standardization, Brussels
23. AIJ (2015) AIJ recommendations for loads on buildings. Architectural Institute of Japan, Tokyo
24. Blackmore PA, Tsokri E (2006) Wind loads on curved roofs. J Wind Eng Ind Aerodyn 94(11):833–844
25. Natalini B, Natalini MB (2017) Wind loads on buildings with vaulted roofs and side walls – A review. J Wind Eng Ind Aerodyn 161:9–16
26. Qiu Y, Sun Y, Wu Y et al (2014) Modeling the mean wind loads on cylindrical roofs with consideration of the Reynolds number effect in uniform flow with low turbulence. J Wind Eng Ind Aerodyn 129:11–21
27. Kumar KS, Stathopoulos T (1998) Power spectra of wind pressure on low building roofs. J Wind Eng Ind Aerodyn 74–76:665–674
28. Li YX, Bai S, Yang QS (2019) Experiment study on non-Gaussian distribution of fluctuating wind load on long-span enclosed cylindrical shell roof. J Build Struct 40(07):62–69
29. Sun Y, Wu Y, Lin ZX et al (2007) Non-Gaussian features of fluctuating wind pressures on long span roofs. China Civ Eng J 40(4):1–5, 12
30. Ye JH, Hou XZ (2010) Non-Gaussian features of fluctuating wind pressures on long span roofs. J Vib Shock 29(7):9–15
31. Wei S, Zhao C, Sun Q (2023) Investigating the non-Gaussian property and its influence on extreme wind pressures on the long-span cylindrical roof. Appl Sci 13(13):7691
32. Chen FB, Zhang T, Yi JR et al (2023) Non-Gaussian characteristics and extreme wind pressure of long-span roof under various approaching flow turbulences. J Build Eng 76:107266
33. Dong X, Ye JH (2010) Conical vortex and its induced wind load on a saddle roof. J Vib Shock 29(10):61–70
34. Wu Y, Wu X, Wei S et al (2021) Experimental study of wind pressure fluctuating characteristics and wind load shape factor of long-span cylinder roof structure. Struct Design Tall Spec Build 30(10):e1860
35. Genesio R, Laurentini A (1960) Tables for Butterworth-digital-filter design. Electron Lett 6(6):157–159
36. Sun Y, Su N, Wu Y (2019) Engineering model of wind pressure spectra on typical large-span roof structures. J Build Struct 40(07):23–33
37. Holmes JD (1979) Mean and fluctuating pressures induced by wind. In: Proceedings of the fifth international conference on wind engineering, Colorado, 8-14 July 1979

Publisher's Note